Constriction Resistance and Current Crowding in Vertical Thin Film Contact

Peng Zhang, *Member, IEEE,* and Y. Y. Lau, *Fellow, IEEE*

***Abstract*—The constriction resistance and the current flow pattern are calculated analytically in a vertical thin film contact in which the thin film base is an equipotential surface. Both Cartesian and cylindrical thin film contacts are studied. The resistivities and the geometric dimensions in the individual contact members may assume arbitrary values. General scaling laws are constructed for the constriction resistance for arbitrary resistivity ratios and geometric aspect ratios. The analytic solutions are validated using a simulation code. Current crowding at the edges is displayed. In the limit of small film thickness, we show that current crowding in the vertical contact is far less serious than the current crowding in the horizontal contact. The data show that the normalized constriction resistance depends predominantly on the geometry of the thin film, but is relatively insensitive to the height and to the resistivity of the member with which the thin film is in contact.**

***Index Terms*—Contact resistance, current crowding, spreading resistance, thin film.**

I. Introduction

Thin film contacts, in which a thin conducting film constitutes at least one of the contacting members, are basic circuit structures in modern electronic devices. They are widely used in micro-electronic and micro-electromechanical systems, and in semiconductor material and device characterization [1], [2]. In miniaturization of electronics, current crowding and Joule heating are important issues [3]–[5].

We consider two basic types of thin film contact: the vertical type [Fig. 1(a)] and the horizontal type [Fig. 1(b)]. In the vertical contact [Fig. 1(a)], the thin film base AB is an equipotential; the current flow is orthogonal to AB, but is tangential to the thin film edges BC and AH. In the horizontal contact [Fig. 1(b)], the thin film edges BC and AH are equipotentials. The current flow is orthogonal to BC and AH, but is tangential to the thin film base AB. As a result, the constriction resistance (also known as the spreading resistance), as well as current crowding at the edges G and D for these two types of thin film contacts are very different.

Manuscript received December 14, 2012; revised April 26, 2013; accepted April 29, 2013. Date of publication May 2, 2013; date of current version July 18, 2013. This work was supported in part by an AFOSR Grant on the Basic Physics of Distributed Plasma Discharge, AFOSR Grant FA9550-09-1-0662, L-3 Communications Electron Devices Division. The review of this paper was arranged by editor C. C. McAndrew.

The authors are with the Department of Nuclear Engineering and Radiological Sciences, University of Michigan, Ann Arbor, MI 48109-2104 USA (e-mail: umpeng@umich.edu; yylau@umich.edu).

Color versions of one or more of the figures in this paper are available online at http://ieeexplore.ieee.org.

Digital Object Identifier 10.1109/JEDS.2013.2261435

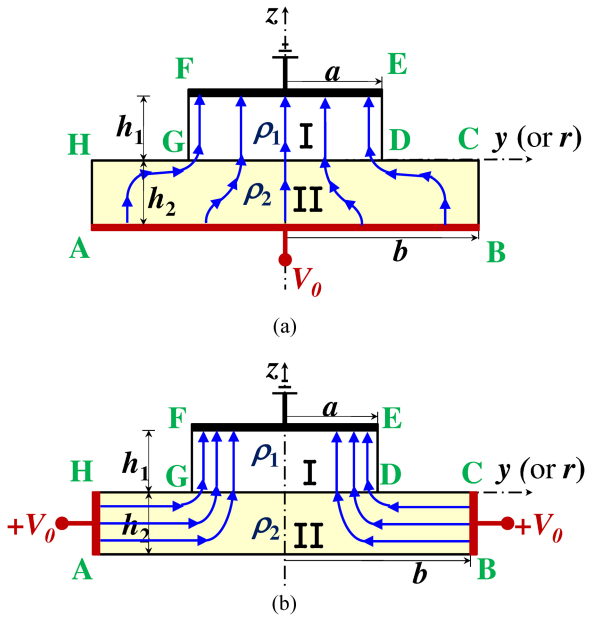

Fig. 1. Two basic types of thin film contact: (a) vertical type, and (b) horizontal type, with dissimilar materials for both Cartesian and cylindrical geometries. For the cylindrical case, the z-axis is the axis of rotation. This paper focuses mainly on the vertical type (a); the horizontal type (b) was solved in [20].

We assume that there are only two contact members, denoted as Region I and Region II, between the electrodes [Figs. 1(a) and (b)]. The interface GD is perfectly smooth and does not contain a resistive sheet.

In this paper, we focus mainly on the vertical contact shown in Fig. 1(a), and provide a comprehensive study of the constriction resistance and the current flows in regions I and II. We point out the marked difference in current crowding at the corners (edges) D and G between vertical contact [Fig. 1(a)] and horizontal contact [Fig. 1(b)]. Without loss of generality, we assume that the top terminal EF is grounded.

The vertical thin film contact has been studied by several authors [6]–[12]. In particular, Hall [6] studied the Cartesian geometry using conformal mapping. Denhoff [12] studied the constriction resistance of a round thin film contact by solving Laplace equation using analytic, numerical, and finite element methods. These studies are restricted to the highly special cases of Fig. 1a: assuming either equal resistivity, $\rho_1 = \rho_2$ [6], or $h_1 \to 0$ [7–9], [12]. We relax these two assumptions in this paper.

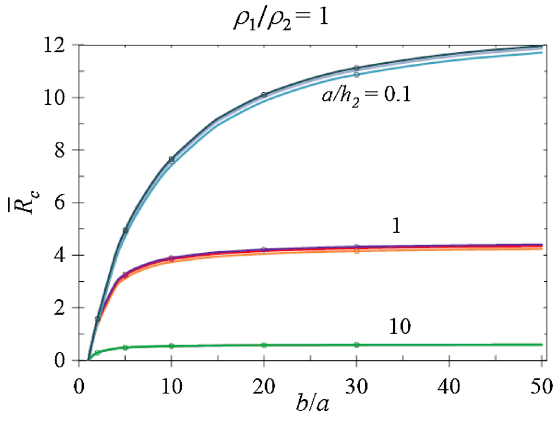

Fig. 2. $\overline{R}_c$ [see (A7)] for Cartesian case as a function of b/a, for $\rho_1/\rho_2 = 1$, $a/h_2 = 0.1$, 1, and 10. For each a/h_2, the three curves are for $h_1/a = 10$, 0.1, and 0.001 (top to bottom). The symbols represent MAXWELL 2-D simulation.

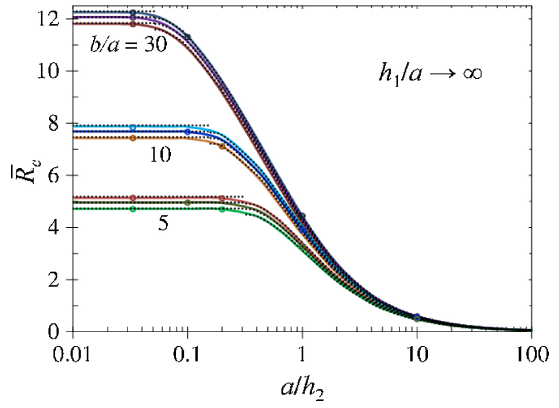

Fig. 3. $\overline{R}_c$ for Cartesian case as a function of a/h_2, in the limit of $h_1/a \to \infty$, for $b/a = 30$, 10, and 5. For each b/a, the three solid curves are for $\rho_1/\rho_2 = 100$, 1, and 0.01 (top to bottom), representing the results from exact calculations [(A7)]. The dotted lines represent (2), and the symbols represent MAXWELL 2-D simulation.

The horizontal thin film contact has also been studied extensively, in both Cartesian [1], [2], [13]–[17] and cylindrical geometry [15]–[19]. Most recently, we treated the 3-terminal horizontal thin film contact in great detail [20], with arbitrary resistivities and geometric dimensions in the individual contact members, as well as arbitrary (unequal) voltages at the terminals BC and AH [Fig. 1(b)]. We found severe current crowding at the edges D and G, for $\rho_1 = 0$, when the thin film thickness h_2 is small [17]. There is a great variety of current crowding in 3-terminal horizontal thin film contact [20].

In both Cartesian and cylindrical geometries [Fig. 1(a)], the resistivities ρ_1 and ρ_2, and the geometric dimensions a, b, h_1, and h_2 may assume arbitrary values. Thus, this paper is applicable to both thin and thick films, and Region I may represent a resistive thin film by letting h_1 small and ρ_1 large. Following the same procedure in studying the bulk contact resistance [21], [22] and the horizontal thin film contacts [15], [20], we analytically solve Laplace equation in Regions I and II of Fig. 1(a), then match the boundary conditions at the contact interface. The potential profile and the constriction resistance are calculated from this exact formulation.

In Section II, we consider the Cartesian vertical thin film contact. We present a formula for the constriction resistance and illustrate the current pattern. We compare our results to those obtained from the MAXWELL 2-D finite element code [23]. In Section III, we consider the cylindrical vertical thin film which is qualitatively similar to the Cartesian solution of Section II. Concluding remarks are given in Section IV. Only the major results will be presented in the main text. Their derivations are given in the appendices.

II. Cartesian Thin Film Vertical Contact

Since the geometry [Fig. 1(a)] is symmetrical about the vertical z-axis, so also are the current flow patterns and the field lines. The field lines are normal to the two terminals AB and EF. The total current is $I = V_0/R$, where R is the resistance between these two terminals, which we find to be

$$R = \rho_1 \frac{h_1}{2a \times W} + \frac{\rho_2}{4\pi W} \overline{R}_c\left(\frac{a}{b}, \frac{h_1}{a}, \frac{a}{h_2}, \frac{\rho_1}{\rho_2}\right) + \rho_2 \frac{h_2}{2b \times W}, \quad (1)$$

where W denotes the channel width in the third ignorable dimension that is perpendicular to the paper. In (1), the first term represents the bulk resistance of Region I. The third term represents the bulk resistance of Region II. The second term represents the remaining constriction (spreading) resistance, R_c, and is expressed as $R_c = \frac{\rho_2}{4\pi W}\overline{R}_c$ for the Cartesian case. The normalized $\overline{R}_c$ depends on the aspect ratios a/b, h_1/a, and a/h_2, and on the resistivity ratio ρ_1/ρ_2, as explicitly shown in (1). The *exact* expression for $\overline{R}_c$ is derived in Appendix A (A7).

If we use the exact expression (A7) in the numerical evaluation of $\overline{R}_c$, we call the result the "exact theory". [In the infinite sum in (A7), we use 10^4 terms; we also use 10^4 terms in the infinite sum in (A3b) to solve for B_n, $n = 1, 2, .., 10^4$.] From the vast amount of data that we collected from the exact theory at various combinations of h_1, h_2, ρ_1, ρ_2, a, and b, we attempted to construct simple fitting formulas for $\overline{R}_c$ so that the values of $\overline{R}_c$, or the bounds of $\overline{R}_c$, may be easily obtained without solving the infinite matrix Eq. (A3b). The bounds on $\overline{R}_c$ are identical to the corresponding asymptotic limits of $\overline{R}_c$, which in some cases (but not all) were solved in the literature by *other* means. Thus, the numerical fitting formulas, given for instance in (2), (3), (5), and (6), are synthesized from a judicious combination of these asymptotic limits, and from the numerical data generated from the exact theory. We validated the exact theory and the synthesized fitting formulas with MAXWELL 2-D simulation codes in Figs. 2, 3, 4, 6, 7, and 8. Similar approaches were used in our recent treatment of the horizontal thin film contact [20].

The exact theory of $\overline{R}_c$ (A7) is plotted in Fig. 2 as a function of b/a, for $\rho_1/\rho_2 = 1$ with various a/h_2 and h_1/a. For a given a/h_2, $\overline{R}_c$ increases as b/a increases. For a/h_2 on the order of 1 or larger, $\overline{R}_c$ approaches almost a constant as b/a becomes large. For a given b/a, $\overline{R}_c$ decreases as a/h_2 increases. The effect of h_1/a on $\overline{R}_c$ is minor. $\overline{R}_c$ increases slightly as h_1/a increases. The effect of h_1/a becomes even less significant as a/h_2 increases.

Since $\overline{R}_c$ is relatively insensitive to h_1/a, in Fig. 3 we plot $\overline{R}_c$ as a function of a/h_2 at various values of b/a and ρ_1/ρ_2, in the

limit of $h_1/a \to \infty$. When $a/h_2 \ll 1$, $\overline{R}_c$ approaches a constant value (independent of h_2) for a given b/a. This is due to the fact that if both h_2 and h_1 become much larger than a, the structure in Fig. 1(a) will become a semi-infinite constriction channel, whose constriction resistance is independent of h_1 and h_2, which was studied in detail in [22]. When $a/h_2>1$, $\overline{R}_c$ decreases as a/h_2 increases. As $a/h_2 \to \infty$, $\overline{R}_c = 2\pi\left(\frac{h_2}{a} - \frac{h_2}{b}\right) \to 0$, which is in sharp contrast to the behavior of the horizontal Cartesian thin film contact studied in [15]–[17], [20], where the current flows parallel to the thin film bottom boundary, and $\overline{R}_c$ (which has a different definition for the horizontal contact [17], [20]) approaches a finite constant of 2.77 as $a/h_2 \to \infty$.

By comparing the data calculated analytically from the exact theory (A7), with the published scalings for some limiting cases [6], [21], [22], [24], we synthesized an accurate, analytical scaling law for the constriction resistance of a general vertical thin film contact, in the $h_1/a \to \infty$ limit,

$$\overline{R}_c\left(\frac{a}{b}, \frac{a}{h_2}, \frac{\rho_1}{\rho_2}\right)\Big|_{h_1/a\to\infty} = \begin{cases} \overline{R}_{c0}\left(\frac{b}{a}\right) + 0.2274 \times \left(\frac{2\rho_1}{\rho_1+\rho_2}\right) \times g\left(\frac{b}{a}\right), & \frac{a}{h_2} < \tan\left(\frac{\pi}{2}\frac{b}{a}\right) \\ p\left(\frac{a}{h_2}\right) \times \left(1 + \frac{0.2274}{q(b/a)} \times \frac{\rho_1-\rho_2}{\rho_1+\rho_2}\right), & \frac{a}{h_2} > \tan\left(\frac{\pi}{2}\frac{b}{a}\right), \end{cases} \tag{2}$$

$$\overline{R}_{c0}(b/a) = 4\ln(2b/\pi a) + 4\ln(\pi/2) \times f(b/a),$$

$$f(b/a) = 0.03250(a/b) + 1.06568(a/b)^2 - 0.24829(a/b)^3 + 0.21511(a/b)^4,$$

$$g(b/a) = 1 - 1.2281(a/b)^2 + 0.1223(a/b)^4 - 0.2711(a/b)^6 + 0.3769(a/b)^8,$$

$$p(a/h_2) = 2\pi(h_2/a) - 4(h_2/a)\tan^{-1}(h_2/a) + 2\ln\left[(h_2/a)^2 + 1\right] - 2\pi(h_2/b),$$

$$q(b/a) = 2\left(\frac{b}{a} + \frac{a}{b}\right)\ln\left(\frac{1+a/b}{1-a/b}\right) + 4\ln\left(\frac{b/a-a/b}{4}\right). \tag{3a-3e}$$

Equation (2) is also plotted in Fig. 3, showing excellent agreement with the exact theory (A7) for arbitrary value of a, $b(>a)$, h_2, ρ_1, and ρ_2, in the limit of $h_1/a \to \infty$.

In (3), $\overline{R}_{c0}(b/a)$, $f(b/a)$, and $g(b/a)$ are derived by Lau and Tang [21], and by Zhang and Lau [(5) and (6) of [22]],[1] $p(a/h_2)$ is derived by Hall [(45) of [6], assuming $\rho_1/\rho_2 = 1$ and $h_1/a \to \infty$], $q(b/a)$ is derived by both Hall [(42) of [6], assuming $\rho_1/\rho_2 = 1$, $h_1/a \to \infty$, and $h_2/a \to \infty$] and Smythe [24]. The breakpoint in (2), $\frac{a}{h_2} = \tan\left(\frac{\pi a}{2b}\right)$, was also stated by Hall [(46) of [6]]. At $\frac{a}{h_2} = \tan\left(\frac{\pi a}{2b}\right)$, there is a discontinuity between the two expressions in (2). This discontinuity at the breakpoint is also seen in the dotted curves in Fig. 3 which plot (2). The size of this step discontinuity is always less than 2% of the exact value of $\overline{R}_c$ [6].

Figure 4(a) shows the exact theory for $\overline{R}_c$ (A7) as a function of ρ_1/ρ_2, for various a/h_2 and h_1/a. Figure 4(b) shows the exact theory for $\overline{R}_c$ (A7) as a function of h_1/a, for various a/h_2 and ρ_1/ρ_2. In both Figs. 4(a) and (b), we fixed $b/a = 30$. In general, as either ρ_1/ρ_2 or h_1/a increases, $\overline{R}_c$ increases. It is important to recognize from Figs. 2–4 that dependence of

[1]An anonymous referee suggested alternate, elegant fitting formulas, $f(x) = 3/[(2x\text{-}1)(2+x)]$, $g(x) = (4/x^2)\,(x^2-1)^2/(4x^2-3)$ where $x = b/a$ (> 1). While these fitting formulas for $f(x)$ and $g(x)$ are not as accurate as (3b) and (3c), they may be used for most practical purposes. We wish to thank this referee for his/her careful reading of the manuscript.

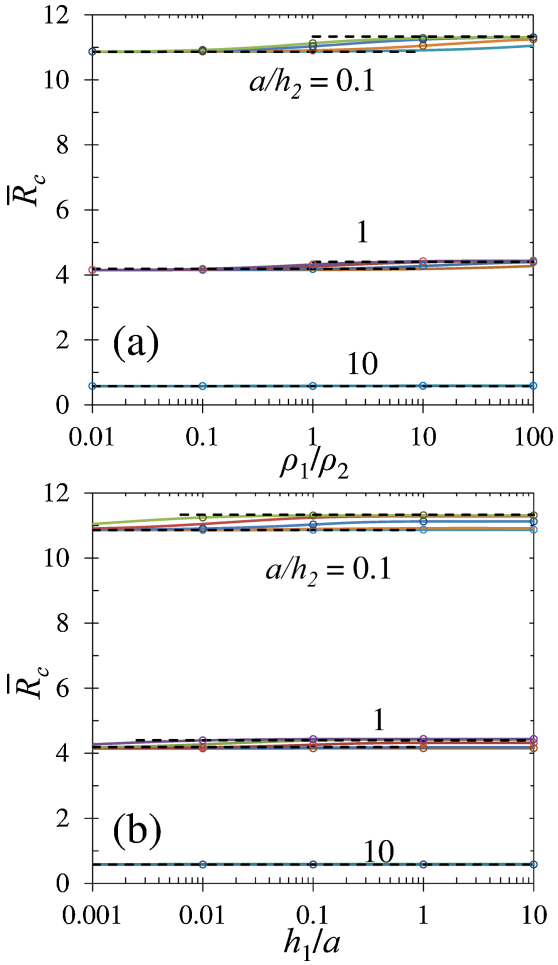

Fig. 4. (a) $\overline{R}_c$ for Cartesian case [see (A7)] as a function of ρ_1/ρ_2, for $a/h_2 = 0.1$, 1, and 10. For each a/h_2, the five solid curves are for $h_1/a = 10$, 1, 0.1, 0.01, and 0.001 (top to bottom), and (b) $\overline{R}_c$ as a function of h_1/a, for $a/h_2 = 0.1$, 1, and 10. For each a/h_2, the five solid curves are for $\rho_1/\rho_2 = 100$, 10, 1, 0.1, and 0.01 (top to bottom). We fixed $b/a = 30$ in all calculations. The dashed lines represent the bounds calculated from (2): for each a/h_2 in (a) and (b), the upper dashed line is calculated from (2) by setting $\rho_1/\rho_2 \to \infty$; the lower dashed line is calculated from (2) by setting $\rho_1/\rho_2 \to 0$. Note that $\rho_1/\rho_2 \to 0$ is equivalent to $h_1/a \to 0$, because in these two limits, the top terminal EF in Fig. 1a is in effect placed directly at the interface DG. The symbols represent MAXWELL 2-D simulation.

$\overline{R}_c$ on h_1/a and on ρ_1/ρ_2 is not significant, and that the major dependence of $\overline{R}_c$ is on a/h_2 and on b/a. Thus, for a given a/h_2 and b/a in Figs. 3 and 4, the bounds of the curves are fairly accurately predicted by (2), which are plotted as dashed lines, for all values of h_1/a and ρ_1/ρ_2.

The field line equation, $y = y(z)$, may be numerically integrated from the first order ordinary differential equation $dy/dz = E_y/E_z = (\partial\Phi/\partial y)/(\partial\Phi/\partial z)$ where Φ is given by (A1). The field lines in the right half of the thin film structure [Fig. 1(a)] are shown in Fig. 5 for the special case of $\rho_1/\rho_2 = 1$, and $h_1/a = 0.01$ with various a/h_2. We set $b/a = 30$ in all calculations in Fig. 5. Note that the variation of a/h_2 in Fig. 5 may be interpreted this way: a, b, and h_1 are held fixed, h_2 decreases, i.e. $h_2 = 5a$, a, and $0.2a$, from Fig. 5(a) to 5(c). (Similar interpretation applies to other figures.) It is clear that as a/h_2 increases, the spreading of the field lines (also the

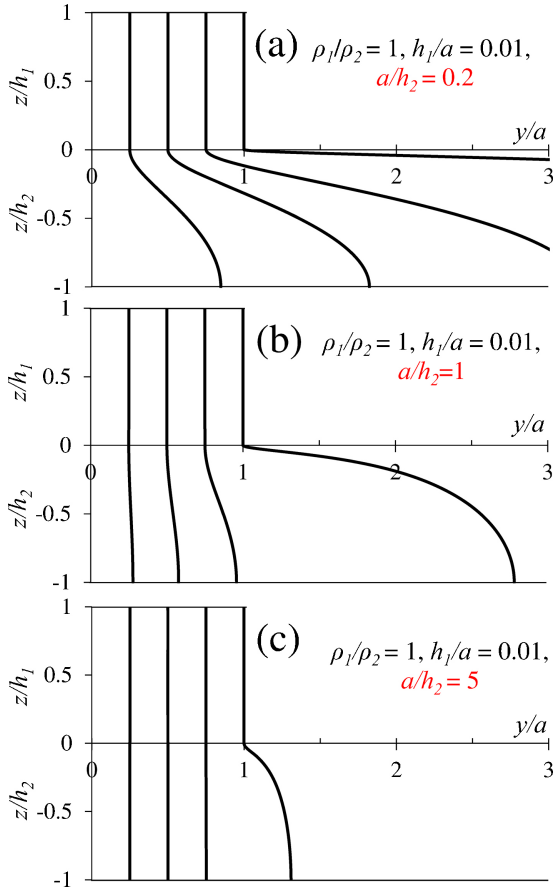

Fig. 5. Field lines calculated from (A1) for the right half of Cartesian thin film contact (Fig. 1a), for the special case of $\rho_1/\rho_2 = 1$ and $h_1/a = 0.01$ with various a/h_2. We fixed $b/a = 30$. The field line distribution is relatively insensitive to h_1/a or ρ_1/ρ_2 (not shown), as compared to the effect of a/h_2.

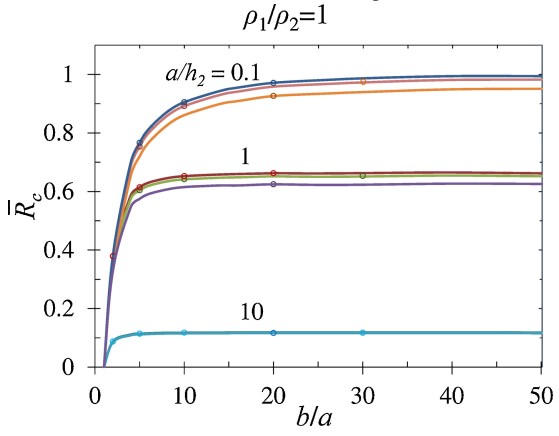

Fig. 6. $\overline{R}_c$ [see (B6)] for cylindrical case as a function of b/a, for $\rho_1/\rho_2 = 1$, $a/h_2 = 0.1$, 1, and 10. For each a/h_2, the three curves are for $h_1/a = 10$, 0.1, and 0.001 (top to bottom). The symbols represent MAXWELL 2-D simulation.

current flow lines) in Region II becomes less significant. This explains the decrease in $\overline{R}_c$ as a/h_2 increases, as shown in Fig. 3. In the limit of $h_2 \to 0$, there will be little spreading of field lines (little current crowding) at the edge of the constriction, leading to zero constriction resistance (Fig. 3), in sharp contrast to the horizontal contact [15], [17], [20]. Note from Fig. 5 that the field lines in Region I are almost straight, and are fairly uniformly spaced across the interface in all the cases, implying minimal enhanced heating at the edges G and D in a vertical contact [Fig. 1(a)]. We also found that

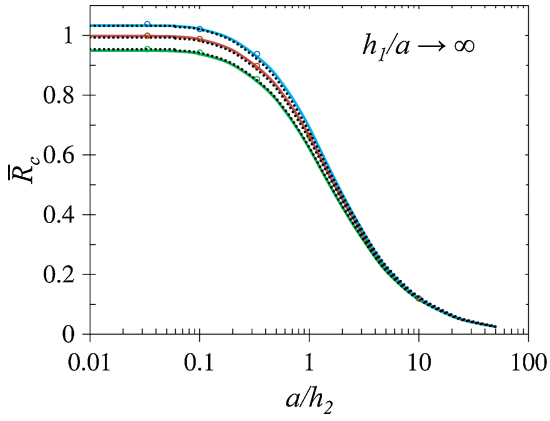

Fig. 7. $\overline{R}_c$ for cylindrical case as a function of a/h_2, in the limit of $h_1/a \to \infty$, for $b/a = 30$, with $\rho_1/\rho_2 = 100$, 1, and 0.01 (top to bottom). The solid lines represent the exact calculations [(B6)], symbols represent MAXWELL 2-D simulation, and the dashed lines represent (5).

as either h_1/a or ρ_1/ρ_2 increases, the spreading of the field lines in Region II slightly increases (not shown). The field line distribution is relatively insensitive to h_1/a or ρ_1/ρ_2, as compared to the effect of a/h_2.

III. Circular Thin Film Vertical Contact

For the circular thin film vertical contact [Fig. 1(a)], the z-axis is the axis of rotation. The total current is $I = V_0/R$, where R is the resistance between the two terminals AB and EF, given by

$$R = \frac{\rho_1 h_1}{\pi a^2} + \frac{\rho_2}{4a}\overline{R}_c\left(\frac{a}{b}, \frac{h_1}{a}, \frac{a}{h_2}, \frac{\rho_1}{\rho_2}\right) + \frac{\rho_2 h_2}{\pi b^2}. \quad (4)$$

In (4), the first and third terms represent the bulk resistance of Region I and II, respectively. The second term represents the remaining constriction resistance, R_c, and is expressed as $R_c = \frac{\rho_2}{4a}\overline{R}_c$ for the circular case. The normalized $\overline{R}_c$ depends on the aspect ratios a/b, h_1/a and a/h_2, and on the resistivity ratio ρ_1/ρ_2, as explicitly shown in (4). The *exact* expression for $\overline{R}_c$ is derived in Appendix B (B6).

The exact theory of $\overline{R}_c$ (B6) is plotted in Fig. 6 as a function of b/a, for $\rho_1/\rho_2 = 1$ with various h_1/a and a/h_2. For a given a/h_2, $\overline{R}_c$ increases as b/a increases. However, $\overline{R}_c$ becomes almost constant for large b/a, independent of the value of a/h_2, which is different from the Cartesian case in Fig. 2, where $\overline{R}_c$ increases logarithmically with b/a if a/h_2 is small [(2a) and (3a)]. For a given b/a, $\overline{R}_c$ decreases as a/h_2 increases. $\overline{R}_c$ increases only slightly as h_1/a increases. The effect of h_1/a becomes even less significant as a/h_2 increases (Fig. 6).

In Fig. 7, we plot $\overline{R}_c$ as a function of a/h_2 for various values of ρ_1/ρ_2, in the limit of $h_1/a \to \infty$. As noted above, $\overline{R}_c$ is independent of b for large b/a; we set $b/a = 30$ for the calculation in Fig. 7. When $a/h_2 \ll 1$, $\overline{R}_c$ approaches a constant value (independent of h_2) for a given b/a. This is due to the fact that if both h_2 and h_1 become much larger than a, the structure in Fig. 1a will become a semi-infinite constriction channel, whose constriction resistance is independent of h_1 and h_2, which was studied in detail in [22].

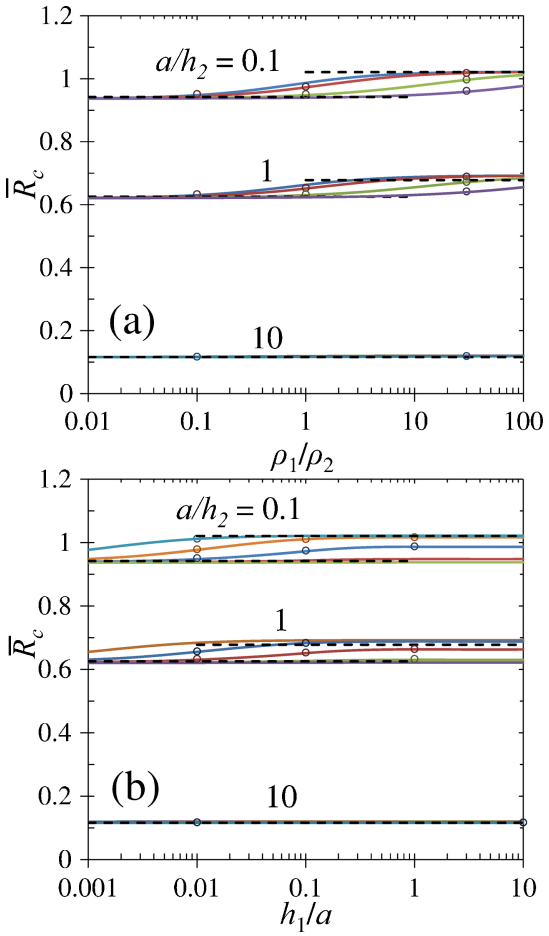

Fig. 8. (a) $\overline{R}_c$ for cylindrical case [see (B6)] as a function of ρ_1/ρ_2, for $a/h_2 = 0.1$, 1, and 10. For each a/h_2, the five solid curves are for $h_1/a = 10$, 1, 0.1, 0.01, and 0.001 (top to bottom), and (b) $\overline{R}_c$ as a function of h_1/a, for $a/h_2 = 0.1$, 1, and 10. For each a/h_2, the five solid curves are for $\rho_1/\rho_2 = 100$, 10, 1, 0.1, and 0.01 (top to bottom). We fixed $b/a = 30$ in all calculations. The dashed lines represent the bounds calculated from (5): for each a/h_2 in (a) and (b), the upper dashed line is calculated from (5) by setting $\rho_1/\rho_2 \to \infty$; the lower dashed line is calculated from (5) by setting $\rho_1/\rho_2 \to 0$. Note that $\rho_1/\rho_2 \to 0$ is equivalent to $h_1/a \to 0$, because in these two limits, the top terminal EF in Fig. 1a is in effect placed directly at the interface DG. The symbols represent MAXWELL 2-D simulation.

When $a/h_2 > 1$, $\overline{R}_c$ decreases as a/h_2 increases. As $a/h_2 \to \infty$, $\overline{R}_c \sim h_2/a \to 0$. This is in sharp contrast to the behavior of the horizontal cylindrical thin film contact studied in [15]–[17], [20], in which the current flows parallel to the thin film bottom boundary, and $\overline{R}_c$ (which has a different definition for the horizontal contact [17], [20]) approaches a finite constant of 0.28 as $a/h_2 \to \infty$.

By comparing the data calculated from the exact theory (B6) with the published scalings for some limiting cases [12], [22], [25], we synthesized an accurate, analytical scaling law for the normalized constriction resistance of a general cylindrical vertical thin film contact, in the $h_1/a \to \infty$ limit, given by Eqs. (5) and (6) at the bottom of this page, where $\Delta = 32/3\pi^2 - 1 = 0.08076$. Equation (5) is also plotted in Fig. 7, showing excellent agreement with the exact theory (B6) for arbitrary value of a, b ($>a$), h_2, ρ_1, and ρ_2, in the limit of $h_1/a \to \infty$.

In (6), $\overline{R}_{c0}(b/a)$ is synthesized by Timsit [25], $g(b/a)$ is derived by us [(3) of [22]], and $p(a/h_2)$ is from Denhoff [(26) and (28) of [12]]. At the breakpoint, $\frac{a}{h_2} = 1.8\frac{a}{b}$ or $\frac{a}{h_2} = \frac{1}{1-(a/b)^2}$, there is a discontinuity between the two expressions in (5). The size of this step discontinuity is within 2% of the exact value of $\overline{R}_c$ (B6) in the worst case.

Figure 8(a) shows the exact theory for $\overline{R}_c$ (B6) as a function of ρ_1/ρ_2, for various a/h_2 and h_1/a. Figure 8(b) shows the exact theory for $\overline{R}_c$ (B6) as a function of h_1/a, for various a/h_2 and ρ_1/ρ_2. Spot checks by MAXWELL 2-D code [23] are also shown in Fig. 8. In general, as either h_1/a or ρ_1/ρ_2 increases, $\overline{R}_c$ increases. It is important to recognize from Figs. 6–8 that the dependence of $\overline{R}_c$ on h_1/a and ρ_1/ρ_2 is not significant, and that the major dependence of $\overline{R}_c$ is on b/a and on a/h_2, similar to the Cartesian case in Section II. Thus, for a given a/h_2 in Fig. 8, the bounds of the curves are fairly accurately predicted by (5), which are plotted as dashed lines.

The field lines for the cylindrical case (not shown) are very similar to those in Fig. 5 for the Cartesian case. In the limit of $h_2 \to 0$, there will be little spreading of field lines (little current crowding) at the edge of the constriction, leading to zero constriction resistance (Fig. 7), in sharp contrast to the horizontal contact [17], [20].

$$\overline{R}_c\left(\frac{b}{a}, \frac{a}{h_2}, \frac{\rho_1}{\rho_2}\right)\Big|_{h_1/a\to\infty} = \begin{cases} \overline{R}_{c0}\left(\frac{b}{a}\right) + \frac{\Delta}{2} \times \left(\frac{2\rho_1}{\rho_1+\rho_2}\right) \times g\left(\frac{b}{a}\right), \\ \quad \text{when} \left[\begin{array}{ll} a/h_2 \le 1.8a/b & \text{if} \quad b/a \ge 4.37, \text{ or} \\ a/h_2 \le \left[1-(a/b)^2\right]^{-1} & \text{if} \quad b/a < 4.37 \end{array}\right]; \\ \left[p\left(\frac{a}{h_2}\right) - \frac{4}{\pi}\left(\frac{a}{b}\right)^2 \frac{h_2}{a}\right] \times \left(1 + \frac{\Delta}{\overline{R}_{c0}(b/a)} \times \frac{\rho_1}{\rho_1+\rho_2}\right), \quad \text{otherwise,} \end{cases} \tag{5}$$

$$\bar{R}_{c0}(b/a) = 1 - 1.41581(a/b) + 0.06322(a/b)^2 + 0.15261(a/b)^3 + 0.19998(a/b)^4,$$
$$g(b/a) = 1 - 0.3243(a/b)^2 - 0.6124(a/b)^4 - 1.3594(a/b)^6 + 1.2961(a/b)^8,$$
$$p(a/h_2) = \begin{cases} [1 + 0.441271\,(a/h_2) + 0.194720\,(a/h_2)^2 - 0.009732\,(a/h_2)^3 \\ -0.046505\,(a/h_2)^4 + 0.002110\,(a/h_2)^5 + 0.052204\,(a/h_2)^6 \\ -0.011044\,(a/h_2)^7]^{-1}, 0 < a/h_2 \le 0.4; \\ 4 \times [0 + 0.31338(h_2/a) - 0.25134(h_2/a)^2 + 0.12512(h_2/a)^3 \\ -0.03436(h_2/a)^4 + 0.003908(h_2/a)^5], 0.4 < a/h_2 < \infty, \end{cases} \tag{6a-6c}$$

IV. Concluding Remarks

This paper presented an exact solution for the constriction resistance in a vertical thin film contact with dissimilar materials, for both Cartesian and cylindrical geometries. The model assumed arbitrary geometric aspect ratios and arbitrary resistivities in the individual contact members. The constriction resistance was calculated analytically, and spot-checked against the MAXWELL 2-D code. The current flow patterns from the exact theory were displayed. Scaling laws for, and bounds on, the constriction resistance were presented for arbitrary values of h_1, h_2, ρ_1, ρ_2, a, and b (>a) [Fig. 1(a)].

We found that the normalized constriction resistance $\overline{R}_c$ depended predominantly on b/a and on h_2/a, i.e., on the geometry of Region II; but was relatively insensitive to h_1/a, and to ρ_1/ρ_2, i.e., insensitive to the geometry or resistivity of Region I [Fig. 1(a)]. We also found that in the limit of small film thickness ($h_2 \to 0$), there was hardly any current crowding in the vertical contact represented in Fig. 1(a). The current was distributed quite uniformly across the interface GD, implying minimal enhanced heating at the edges G and D in Fig. 1(a). This was in sharp contrast to a horizontal thin film contact [Fig. 1(b)], where the current that crosses the interface GD was highly concentrated near the edges G and D. In fact, at least half of the current flew within a distance of 0.44 h_2 ($h_2 \to 0$ [17]) of the two edges G and D in Fig. 1(b), suggesting severe local heating there for the horizontal thin film contact.

Appendix A

General Solution to the Cartesian Vertical Contact [Fig. 1(a)]

The formulation follows that of [15], [20], and [22]. Referring to Fig. 1(a), EF is grounded, and AB is biased with a voltage of $+V_0$. The solutions to Laplace's equation are,

$$\begin{aligned}\Phi_+(y,z) &= A_0(z-h_1) + \sum_{n=1}^{\infty} A_n \cos\left(\tfrac{n\pi y}{a}\right) \sinh\left(n\pi \tfrac{z-h_1}{a}\right),\\ &\quad 0 < z < h_1,\ |y| \in (0,a),\\ \Phi_-(y,z) &= V_0 + B_0(z+h_2) + \sum_{n=1}^{\infty} B_n \cos\left(\tfrac{n\pi y}{b}\right) \sinh\left(n\pi \tfrac{z+h_2}{b}\right),\\ &\quad -h_2 < z < 0,\ |y| \in (0,b),\end{aligned} \tag{A1}$$

where Φ_+ and Φ_- are the electrical potential in the regions I and II respectively, and A_n and B_n are the coefficients that need to be determined.

At the interface $z=0$, from the continuity of electrical potential and current density, we have the following boundary conditions

$$\Phi_+ = \Phi_-, \qquad z=0,\ |y| \in (0,a) \tag{A2a}$$

$$\frac{1}{\rho_1}\frac{\partial \Phi_+}{\partial z} = \frac{1}{\rho_2}\frac{\partial \Phi_-}{\partial z}, \qquad z=0,\ |y| \in (0,a), \tag{A2b}$$

$$\frac{\partial \Phi_-}{\partial z} = 0, \qquad z=0,\ |y| \in (a,b) \tag{A2c}$$

From (A1) and (A2a), eliminating coefficient A_n in favor of B_n, we have

$$-A_n \sinh\left(n\pi\frac{h_1}{a}\right) = \sum_{m=1}^{\infty} g_{mn} B_m \sinh\left(m\pi\frac{h_2}{b}\right), \tag{A3a}$$

$$\begin{aligned}&\frac{\rho_1}{\rho_2} n B_n \cosh\left(n\pi\frac{h_2}{b}\right) + \sum_{m=1}^{\infty} \gamma_{nm} B_m \sinh\left(\frac{m\pi h_2}{b}\right)\\ &\quad = \frac{2}{\pi}\frac{\sin(n\pi a/b)}{n\pi a/b}, \qquad n = 1, 2, 3...\end{aligned} \tag{A3b}$$

where

$$\begin{aligned}\gamma_{nm} = \gamma_{mn} &= \sum_{l=1}^{\infty} l g_{nl} g_{ml} \coth\left(\frac{l\pi h_1}{a}\right),\\ g_{mn} &= \frac{2}{a}\int_0^a dy \cos\left(\frac{m\pi y}{b}\right)\cos\left(\frac{n\pi y}{a}\right).\end{aligned} \tag{A4}$$

In deriving (A3b), we have assumed that $aA_0 = +1$. The infinite matrix in (A3b) can be solved directly for B_n with convergence guaranteed [22], from which A_n follows in (A3a).

The total current from AB to EF is, [Fig. 1(a)]

$$I = 2W\int_0^a \frac{1}{\rho_1}\left.\frac{\partial \Phi_+}{\partial z}\right|_{z=0} dy = \frac{2W}{\rho_1}, \tag{A5}$$

where we have used (A1) and $aA_0 = +1$, and W is the width in the third, ignorable dimension that is perpendicular to the paper. The terminal voltage V_0 may be expressed in terms of B_n as

$$V_0 = -\frac{h_1}{a} - B_0 h_2 - \frac{1}{a}\sum_{n=1}^{\infty} B_n \sinh\left(\frac{n\pi h_2}{b}\right)\frac{\sin(n\pi a/b)}{n\pi a/b} \tag{A6}$$

We found $B_0 = (\rho_2/\rho_1)/b$, after taking $\partial\Phi_-/\partial z$ in (A1) and using (A2b) and (A2c) in the resultant Fourier series.

The constriction resistance, R_c, is defined as the difference between the resistance from AB to EF, $R = V_0/I$, and the bulk resistance, $R_u = \rho_1 h_1/2aW + \rho_2 h_2/2bW$,

$$\begin{aligned}&R_c \equiv \tfrac{\rho_2}{4\pi W}\overline{R}_c = \tfrac{V_0}{I} - R_u,\\ &\bar{R}_c = \bar{R}_c\left(\tfrac{a}{b}, \tfrac{h_1}{a}, \tfrac{a}{h_2}, \tfrac{\rho_1}{\rho_2}\right) = 2\pi\tfrac{\rho_1}{\rho_2}\sum_{n=1}^{\infty} B_n \sinh\left(\tfrac{n\pi h_2}{b}\right)\tfrac{\sin(n\pi a/b)}{n\pi a/b}.\end{aligned} \tag{A7}$$

Equation (A7) is the *exact* expression for the constriction resistance of Cartesian vertical thin film contact [Fig. 1(a)] for arbitrary values of a, b (b>a), h_1, h_2 and ρ_1/ρ_2. In (A7), B_n is solved from (A3b). Equation (A7) appears in (1) of the main text.

APPENDIX B

General Solution to the Circular Vertical Contact [Fig. 1(a)]

The solutions to Laplace's equation in cylindrical geometry are [15], [20], [22],

$$\begin{aligned}\Phi_+(r,z) &= A_0(z-h_1)+\sum_{n=1}^{\infty}A_nJ_0(\alpha_nr)\sinh[\alpha_n(z-h_1)],\\ &\quad 0<z<h_1, r\in(0,a);\\ \Phi_-(r,z) &= V_0+B_0(z+h_2)+\sum_{n=1}^{\infty}B_nJ_0(\beta_nr)\sinh[\beta_n(z+h_2)],\\ &\quad -h_2<z<0, r\in(0,b),\end{aligned}\tag{B1}$$

where Φ_+ and Φ_- are the electrical potential in the regions I and II, respectively, α_n and β_n satisfy $J_1(\alpha_n a)=J_1(\beta_n b)=0$, $J_0(x)$ and $J_1(x)$ are the Bessel functions of order zero and one respectively, and A_n and B_n are the coefficients that need to be determined.

At the interface $z=0$, from the continuity of electrical potential and current density, we have the following boundary conditions:

$$\Phi_+=\Phi_-,\qquad z=0, r\in(0,a),\tag{B2a}$$

$$\frac{1}{\rho_1}\frac{\partial\Phi_+}{\partial z}=\frac{1}{\rho_2}\frac{\partial\Phi_-}{\partial z},\qquad z=0, r\in(0,a),\tag{B2b}$$

$$\frac{\partial\Phi_-}{\partial z}=0,\qquad z=0, r\in(a,b)\tag{B2c}$$

From (B1) and (B2a), the coefficient A_n is expressed in terms of B_n,

$$-A_0h_1=\sum_{n=1}^{\infty}B_n\sinh(\beta_nh_2)\frac{2J_1(\beta_na)}{\beta_na}+V_0+B_0h_2,\tag{B3a}$$

$$\begin{aligned}-\sinh(\alpha_nh_1)A_n &= \sum_{m=1}^{\infty}B_m\sinh(\beta_mh_2)\,g_{mn},\\ g_{mn} &= \frac{2}{a^2J_0^2(\alpha_na)}\int_0^a rdrJ_0(\alpha_nr)\,J_0(\beta_mr),\ n\geq 1.\end{aligned}\tag{B3b}$$

Combining (B2b), (B2c) and (B3b), we obtain

$$\begin{aligned}&\frac{\rho_1}{\rho_2}\frac{b}{a}\beta_nbJ_0^2(\beta_nb)\cosh(\beta_nh_2)B_n+\sum_{m=1}^{\infty}\gamma_{nm}B_m\sinh(\beta_mh_2)\\ &\quad=\frac{2J_1(\beta_na)}{\beta_na},\qquad n=1,2,3...,\end{aligned}\tag{B4}$$

where

$$\gamma_{nm}=\gamma_{mn}=\sum_{l=1}^{\infty}g_{nl}g_{ml}\alpha_laJ_0^2(\alpha_la)\coth(\alpha_lh_1),\tag{B5}$$

and g_{nl} and g_{ml} is in the form of the last part in (B3b). In deriving (B4), we have set $aA_0=1$ for simplicity.

The total resistance from AB to EF is $R=V_0/I$, where $I=\int_0^a\left(\frac{1}{\rho_1}\left.\frac{\partial\Phi_+}{\partial z}\right|_{z=0}\right)2\pi rdr=\pi a/\rho_1$ is the total current from AB to EF [Fig. 1(a)], and V_0 can be found from (B3a) with $B_0=(\rho_2/\rho_1)\,a/b^2$. This expression for B_0 is obtained after taking $\partial\Phi_-/\partial z$ in (B1) and using (B2b) and (B2c) in the resultant Fourier series.

The constriction resistance, R_c, is the difference between the total resistance R and the bulk resistance $R_u=\rho_1h_1/\pi a^2+\rho_2h_2/\pi b^2$. We find

$$\begin{aligned}R_c &\equiv \frac{\rho_2}{4a}\overline{R}_c=\frac{V_0}{I}-R_u,\\ \bar{R}_c\left(\frac{a}{b},\frac{h_1}{a},\frac{a}{h_2},\frac{\rho_1}{\rho_2}\right) &= \frac{8}{\pi}\frac{\rho_1}{\rho_2}\sum_{n=1}^{\infty}B_n\sinh(\beta_nh_2)\frac{J_1(\beta_na)}{\beta_na},\end{aligned}\tag{B6}$$

which is the *exact* expression for the circular vertical thin film constriction resistance with dissimilar materials for arbitrary values of a, b (b>a), h_1, h_2 and ρ_1/ρ_2. In (B6), B_n is solved from (B4). Equation (B6) appears in (4) of the main text.

ACKNOWLEDGEMENTS

We thank Derek Hung for help in data collection.

REFERENCES

[1] H. H. Berger, "Models for contacts to planar devices," *Solid State Electron.*, vol. 15, no. 2, pp. 145–158, Feb. 1972.
[2] D. K. Schroder, *Semiconductor Material and Device Characterization*, 2 ed., New York, NY, USA: Wiley, 1998, p. 149.
[3] D. Hyman and M. Mehregany, "Contact physics of gold microcontacts for MEMS switches," *IEEE Trans. Compon. Packag. Technol.*, vol. 22, no. 3, pp. 357–364, Sep. 1999.
[4] F. Léonard and A. A. Talin, "Electrical contacts to one- and two-dimensional nanomaterials," *Nature Nanotech.*, vol. 6, no.12, pp. 773–783, Nov. 2011.
[5] Y. Khatami, H. Li, C. Xu, and K. Banerjee, "Metal-to-Multilayer-Graphene Contact—Part I: Contact Resistance Modeling," *IEEE Trans. Electron Devices*, vol. 59, no. 9, pp. 2444–2452, Dec. 2012.
[6] P. M. Hall, "Resistance calculations for thin film patterns," *Thin Solid Films*, vol. 1, no. 4, p. 277, 1967.
[7] S. Kristiansson, F. Ingvarson, and K. O. Jeppson, "Compact spreading resistance model for rectangular contacts on uniform and epitaxial substrates," *IEEE Trans. Electron. Devices*, vol. 54, no. 9, pp. 2531–2536, Sep. 2007.
[8] A. Nussbaum, "Capacitance and spreading resistance of a stripe line," *Solid-State Electron.,* vol. 38, no. 6, pp. 1253–1256, 1995.
[9] M. S. Leong, S. C. Choo, and L. S. Tan, "The role of source boundary condition in spreading resistance calculations," *Solid-State Electron.*, vol. 21, no. 7, pp. 933–941, 1978.
[10] R. H. Cox and H. Strack, "Ohmic contacts for GaAs devices," *Solid-State Electron.*, vol. 10, no. 12, pp. 1213–1218, 1967.
[11] B. Gelmont and M. Shur, "Spreading resistance of a round ohmic contact," *Solid-State Electron.*, vol. 36, no. 2, pp. 143–146, 1993.
[12] M. W. Denhoff, "An accurate calculation of spreading resistance," *J. Phys. D: Appl. Phys.*, vol 39, no. 9, pp. 1761–1765, 2006.
[13] H. Murrmann, and D. Widmann, "Current crowding on metal contacts to planer devices," *Dig. Tech. Pap. ISSCC*, vol. XII, no. 12, pp. 162–163, 1969.
[14] D. P. Kennedy and P. C. Murley, "A Two-Dimensional Mathematical Analysis of the Diffused Semiconductor Resistor," *IBM J. Res. Develop.*, vol. 12, no. 3, pp. 242–250, 1968.
[15] P. Zhang, Y. Y. Lau, and R. M. Gilgenbach, "Thin film contact resistance with dissimilar materials," *J. Appl. Phys.*, vol. 109, no. 12, p. 124910, 2011.
[16] P. Zhang, Y. Y. Lau, and R. M. Gilgenbach, "Minimization of thin film contact resistance," *Appl. Phys. Lett.*, vol. 97, no. 20, p. 204103, 2010.
[17] P. Zhang, Y. Y. Lau, and R. S. Timsit, "On the spreading resistance of thin-film contacts," *IEEE Trans. Electron Devices*, vol. 59, no. 7, pp. 1936–1940, Jul. 2012.

[18] G. Norberg, S. Dejanovic, and H. Hesselbom, "Contact resistance of thin metal film contacts," *IEEE Trans. Compon. Packag. Technol.*, vol. 29, no. 2, pp. 371–378, Jun. 2006.
[19] R. Timsit, "Constriction resistance of thin-film contacts," *IEEE Trans. Compon. Packag. Technol.*, vol. 33, no. 3, pp. 636–642, Sep. 2010.
[20] P. Zhang, D. Hung, and Y. Y. Lau, "Current flow in a 3-terminal thin film contact with dissimilar materials and general geometric aspect ratios," *J. Phys. D: Appl. Phys.*, vol. 46, no. 6, p. 065502, 2013; Corrigendum, ibid, vol. 46, p. 209501, 2013.
[21] Y. Y. Lau and W. Tang, "A higher dimensional theory of electrical contact resistance," *J. Appl. Phys.*, vol. 105, no. 12, p. 124902, 2009.
[22] P. Zhang and Y. Y. Lau, "Scaling laws for electrical contact resistance with dissimilar materials," *J. Appl. Phys.*, vol. 108, no. 4, p. 044914, 2010. (There was a typo in this paper. In equation (6) of this paper, the term -2.2281$(a/b)^2$ in $g(b/a)$ should read -1.2281$(a/b)^2$).
[23] "MAXWELL software.'' [Online] Available:http://www.ansoft.com
[24] W. R. Smythe, *Static and Dynamic Electricity*, 2nd Ed. New York, NY, USA: McGraw Hill, 1950, p. 237.
[25] R. Timsit, "Electrical contact resistance: Properties of stationary interfaces," *IEEE Trans. Compon. Packag. Technol.*, vol. 22, no. 1, pp. 85–98, Mar. 1999.

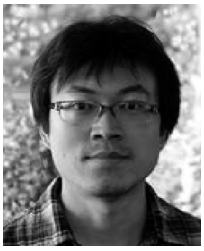

Peng Zhang (S'07–M'12) received the B.Eng and M.Eng degrees in electrical and electronic engineering from Nanyang Technological University, Singapore in 2006 and 2008, respectively, and the Ph.D. degree in nuclear engineering and radiological sciences from the University of Michigan at Ann Arbor, Michigan, USA, in 2012. He has authored or co-authored more than a dozen refereed journal articles on electrical contacts, surface roughness-induced heating, surface flashover and discharge, relativistic magnetron, classical and quantum diodes, magneto-Rayleigh-Taylor instability, and laser-solid interaction.

He was a recipient of the 2012 IEEE Nuclear and Plasma Sciences Graduate Scholarship Award.

Y. Y. Lau (M'98–SM'06–F'08) received the S.B., S.M., and Ph.D. degrees in electrical engineering from the Massachusetts Institute of Technology (MIT), Cambridge, MA, USA, in 1968, 1970, and 1973, respectively.

From 1973 to 1979, he had been an Instructor and then an Assistant Professor in applied mathematics at MIT. He was with Science Applications Inc., McLean, VA, USA, from 1980 to 1983, and with the Naval Research Laboratory (NRL), Washington, DC, USA, from 1983 to 1992, both as a Research Physicist. In 1992, he joined the University of Michigan, Ann Arbor, as a Professor in the Department of Nuclear engineering and Radiological Sciences, and in the Applied Physics Program. He has worked on electron beams, coherent radiation sources, plasmas and discharges. He has over 190 refereed publications and 10 patents.

He served three terms as an Associate Editor of the *Physics of Plasmas*, and was a Guest Editor of the IEEE TRANSACTIONS ON PLASMA SCIENCE Special Issue on high-power microwave generation. While at the NRL, he was a recipient of several Invention and Publication Awards and the 1989 Sigma-Xi Scientific Society Applied Science Award. He became a fellow of the American Physical Society in 1986, an IEEE Fellow in 2008 and was the recipient of the 1999 IEEE Plasma Science and Applications Award.